Characterization Of Nano-Second Laser Induced Plasmas From Al Target In Air At Atmospheric Pressure

H. Hegazy[a], F. M. Abdel-Rahim[b], A. M A. Nossair[b] S. H. Allam[c] and Th. M. El-Sherbini[c]

a) Plasma Physics Dept., N.R.C, Egyptian Atomic Energy Authority, 13759 Enshass, Egypt
b) Physics Dept., Faculty of Science, Al- Azhar University, Assuit Branch, Egypt.
c) Lab. of Lasers and New Materials, Dept. of Physics, Faculty of Science, Cairo Uni., Cairo, Egypt.

Abstract. In the present work we study the effect of the laser beam energy on the properties of the plasma generated by focusing an intense laser beam on Al solid target in air at atmospheric pressure. Plasma is generated using a Nd:YAG pulsed laser at 1064 nm wavelength, 6 ns pulse duration with a maximum pulse energy of 750mJ. The emission spectrum is collected using an Echelle spectrometer equipped with ICCD camera Andor type. The measurements were performed at several delay times between 0 to 9μs. Measurements of temperature and electron density of the produced plasmas at different laser energies and at different delay times are described using different emission spectral lines. Based on LTE assumption, excitation temperature is determined from the Boltzmann plot using O I spectral lines at 777.34*, 794.93, and 848.65 nm* and the electron density is determined from Stark width of Al II at 281.6 and 466.3 nm. The determined density is compared with the density determined from H_α spectral line.

Keywords: Laser-plasma interactions, Laser-produced plasma, laser-plasma interactions of solids.
PACS: 52.38.-r, 52.50.Jm, 79.20.Ds

INTRODUCTION

Laser-induced plasma spectroscopy (LIPS), is being used as an analytical method by a growing number of research groups [1-4]. The growing interest in LIPS, particularly in the last ten years, has led to an increasing number of publications on its applications, both in the laboratory and in industry. Laser-induced plasmas at low flounce (typically 10 J/cm^2) have various applications such as pulsed laser deposition (PLD) or multi-elemental analysis. Technique of the latter depends on analyzing the light spectrum emitted from the plasma created at the sample surface by means of laser pulses, most of the time in the presence of ambient gas. LIPS has many practical advantages over more conventional elemental analysis techniques and is consequently being considered for a growing number of applications [5,6] including on-line process or in situ analysis. A more detailed description of this technique and its main characteristics can be found elsewhere [7-9]. Many of these publications deal with the experimental investigation of the influence of the pulse duration on the plasma characteristics, whereas others are related to a plasma model predicting the dependence of target ablation and plasma properties on laser conditions. Because the assumption of local thermodynamic equilibrium (LTE) condition is essential to characterize the plasma, a specific experimental study has also been devoted to this question [10].

*** Corresponding author: Tel. 0020101980955, Fax. 0220882325647**

E-mail: farid.elkhateb@gmail.com (F. M. Abdel-Rahim)

The aim of the present work is to investigate the thermal behavior of the laser produced plasma. The investigation is devoted to Study the effect of laser energy on the plasma produced by incidence of nano-second laser beam on Al target in air at atmospheric pressure and at different delay times.

The determinations of temperature and electron density are usually considered to be the most important parameters to characterize the state of produced plasma. An accurate knowledge of both leads to understand the processes taking place in the plasma such as vaporization, dissociation, ionization and excitation.

EXPERIMENTAL SET-UP

The present work was performed using the experimental setup shown in fig. (1). A Q-switched Nd-YAG Brilliant laser from Quantel delivering 750 mJ in 6 ns FWHM at the fundamental wavelength 1.06μm was used. The energy per pulse was 670 mJ at the target surface, which corresponds to 5.6 x10^{10} W/cm^2 for a laser focal spot radius of 0.25 mm. The laser was focused onto the target using 10 cm quartz lens. The incident power on the target was monitored using an absolutely calibrated power meter in conjunction with a plane quartz beam splitter reflecting 5% of the incident laser beam. A certified reference aluminum alloy sample 316 Alusuisse of known elemental composition was used in the present experiment. The Al target is firstly polished and for

CP1047, *Laser and Plasma Applications in Materials Science,* edited by E.-H. Amara, S. Boudjemai, and D. Doumaz

each laser shot the target is moved so a fresh surface is provided.

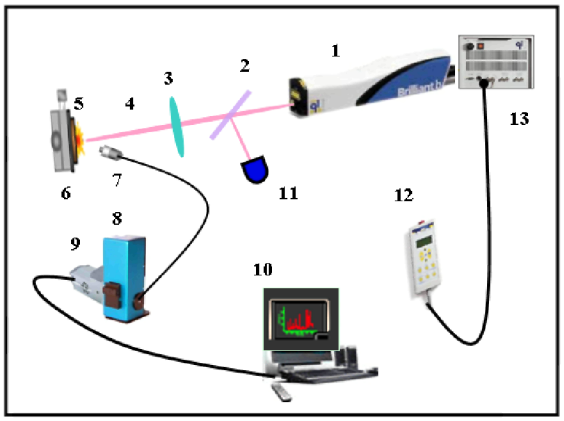

FIGURE 1. A schematic diagram of experimental setup. 1. Nd:YAG Laser 2.Laser Beam Splitter 3. Quartz Lens 4. Laser Beam 5.Plasma Plume 6. Al Target 7. Optical Fiber 8. Echlle Spectrograph 9. ICCD Camera 10. PC 11. Power Meter 12. Remote Control 13. Power Supply.

The emission spectrum was recorded using a SE 200 Echelle spectrograph produced by Catalina corporation. equipped with an ICCD type Andor model iStar DH734-18F. The gain of the camera was fixed at a value of 250 with binning mode at 1x1. This spectrometer allows for a time resolved spectral acquisition over the whole UV-NIR (200-1000nm) with a constant resolution $\Delta\lambda/\lambda$=4500 over three points. An Oriel low pressure Hg lamp was used for wavelength calibration. A quartz fiber cable of diameter 25 μm was employed to conduct the emitted light from the plasma plume to the entrance hole of the Echelle spectrograph. The fiber tip was positioned using a x-y translational stage of a resolution of 100 μm, which enabled us to fix the fiber at 1.25 cm from the laser axis at a distance of 1.5 mm normal to the target. The cross sectional area seen by the fiber was estimated by feeding a laser beam from the backside of the fiber using a small diode laser. The estimated cross sectional area was 2 ± 0.1 mm. The spectra were acquired at different delays after the laser pulse, using constant opening gates of ICCD. The choice of the gate corresponds to a compromise between the need of not having very large variations of the signal during the measurement time, and at the same time having a good signal for calculating line intensities and widths. The experimental results were collected from three single shots at three fresh target positions for checking the reproducibility; this allows us to present an average and a standard deviation of the results.

RESULTS AND DISCUSSIONS

The present measurements are done for different laser energies (95-670 mJ) and different delay times (0-9μs) for the fundamental laser wavelength (1.064 μm).

Figure (2) shows the emission spectrum of the produced plasma in the spectral range 200-900 nm for different laser energies between 670 and 130 mJ, and at a delay time of 1 μs .

The data taken was spatially integrated from the surface of the target up to 2 mm normal to the target surface. This confirms that the plasma is homogenous within this short distance in front of the target. [11-13]
The continuum emission decreases quickly with increasing delay time because of the expansion of the plasma. The intensities of lines can last for up to several microseconds.

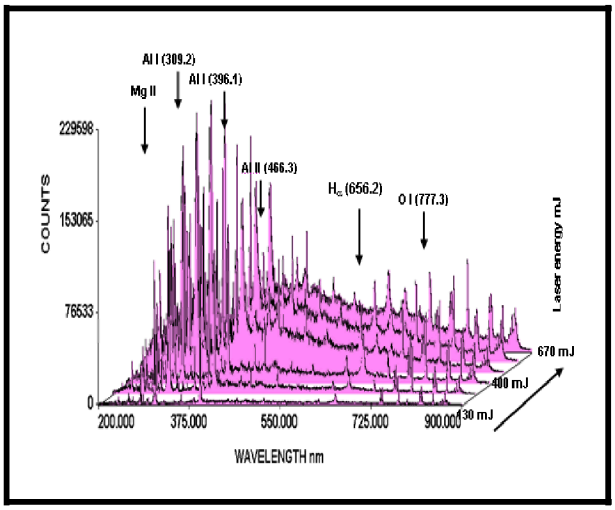

FIGURE 2. Collected emission spectrum from the produced plasma in the spectral range 200-900 nm for different laser energies (670 mJ and 130 mJ) and at a delay time of 1 μs.

These time intervals are much longer than the lifetime of the excited state of the Al atoms, so it can be concluded that Al atoms are excited constantly while revealing to the laser source, and that the exciting energy comes from the plasma life time itself (≤ 30 μs).

The excitation temperature can be determined from the measurement of the intensity of the spectral lines assuming that the population of the energy levels follows the Boltzmann distribution law. For full LTE the intensity of a spectral line is given by

$$I_{ij} = \frac{L}{4\pi} h\nu\, g_i\, A_{ij}\, \frac{N_\circ}{U(T)}\, \exp\left\{ - \frac{E_i}{k_B T_{exc}} \right\} \quad (1)$$

Where L is the plasma length, N_o is the number density of atoms in the ground state, U(T) is the partition function, T_{exc} is the excitation temperature ≈ electron temperature, E_i is the excitation energy of the upper level, A is transition probability, g is statistical Wight and k_B Boltzmann constant .

The plasma temperature calculated is developed from Boltzmann plot using the three O I spectral lines at the wavelengths 777.34, 794.93, and 848.65 nm. These spectral lines were previously tested and proved they to be suitable for the temperature calculates of the laser produced plasmas in air.[14] Figure (3) presents the obtained Boltzmann plots at different laser energies with good regression (~ 0.999).

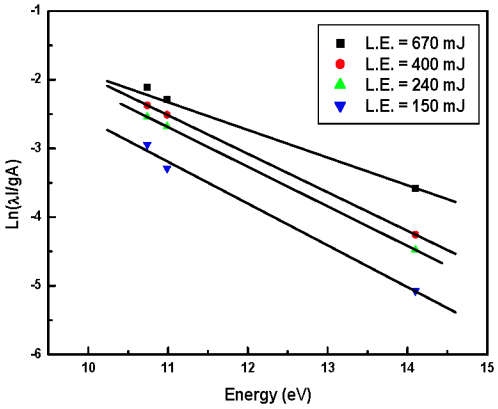

FIGURE 3. Boltzmann plot for different laser energies.

Figure 4. shows the variation of the excitation temperature with the delay time for different laser energies. However Figure 5. presents the variation of the calculated excitation temperature versus different laser energies and for different delay times.

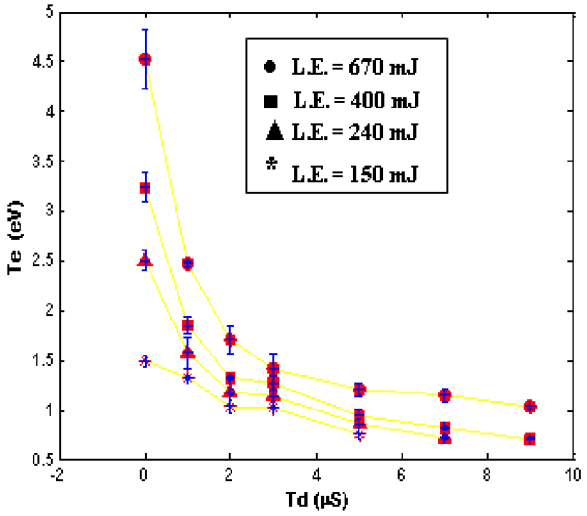

FIGURE 4. Variation of the excitation temperature (T_{exc}) calculated for versus different delay times, and for different laser energies.

Samples of the results in the figures (Fig.(4), Fig.(5)) shown in the following table (1). The excitation temperature T_{exc} decreases quickly with delay time. After the end of laser pulse, the atoms in plasma are excited while leaving the target surface and traveling in the direction of laser source. Moreover, the impact excitation after the end of the laser pulse is the dominant process in the plasma and it is cooling. As well as higher laser irradiance gives rise to more target heating, melting and vaporization, also resulting a higher vapor density, velocity and temperature in the plume, and more charged species as expected.

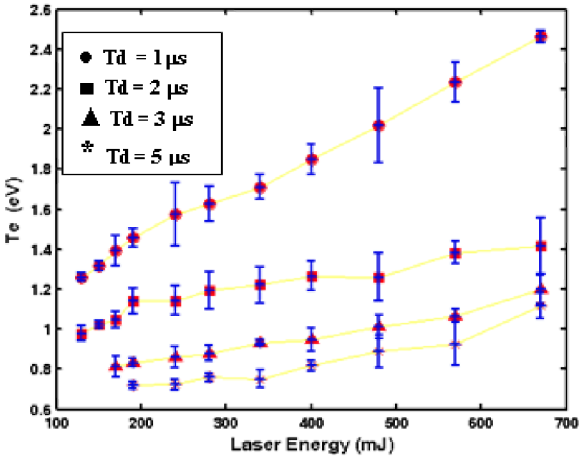

FIGURE 5. Variation of the excitation temperature (T_{exc}) calculated for versus different laser energies and for different delay times.

TABLE 1. the results excitation temperature (eV) at different delay times and different laser energies.

L.E. / Td	670mJ	400mJ	240mJ	150mJ
1 μs	**2.46** ± 0.029	**1.80** ± 0.076	**1.57** ± 0.15	**1.38** ± 0.025
2 μs	**1.70** ± 0.15	**1.32** ± 0.014	**1.18** ± 0.034	**1.03** ± 0.066
3 μs	**1.42** ± 0.14	**1.26** ± 0.07	**1.19** ± 0.072	**1.14** ± 0.020
5 μs	**1.20** ± 0.07	**0.95** ± 0.056	**0.86** ± 0.050	**0.75** ± 0.055

One of the important parameters for understanding the thermal behavior of the produced plasma by laser is the electron density. In the present work electron density is determined from the Stark broadening of different spectral lines such as Al II-line at 281.62 nm and 466.3 nm, and the obtained result is compared with that determined from the Stark width of H_α spectral line which had been previously proved to be a good test for comparison of experiments the same typical conditions [11].

Spectral line broadening in plasma is affected mainly by two physical mechanisms namely; Doppler broadening and Pressure broadening. In the present work because of the plasma produced by laser reveals low temperatures (≤ 2 eV) and high densities (10^{18} cm^{-3}), the contributions by Doppler, Van der Waals, and resonance broadenings are neglected for the Al II spectral lines at 281.6 nm and 466.3 nm which had been used to determine the electron density. The Stark width parameter (w) of these lines had been accurately determined experimentally by Colon et al.[13] as:

$$\Delta\lambda_{1/2} = 2w\left(\frac{N_e}{10^{16}}\right) \qquad (2)$$

Extraction of Stark width of Al II spectral lines in the present study is proceeded as follows; the instrumental function was convoluted with a Lorentzian function of variable width and

fitted to the experimental profile by a least-square fitting procedure yielding the collisional contribution to the width of the line profile. However, the measured instrumental width is found to be 0.12 nm (determined by measuring the FWHM of the Hg lines emitted by a standard low pressure Hg lamp as mentioned in experimental setup section).

Figure (6) a and b show the typical profile of Al II spectral line at 466.3 nm and 281.63 nm with their final fitted profiles.

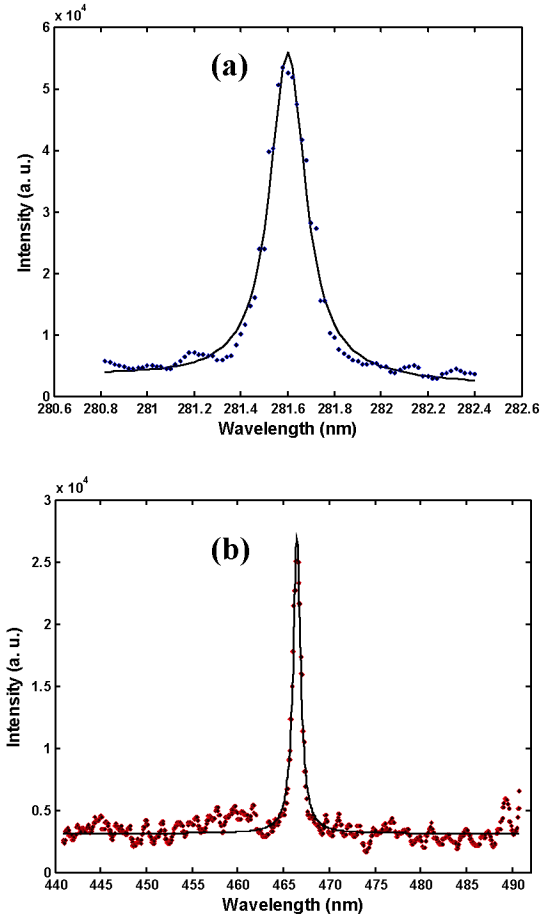

FIGURE 6. Spectral profile of (a) Al II at 281.6nm and (b) Al II at 466.3nm with its least square fit (solid line).

For the Al II-line at 281.62 nm, the parameter (w_{ref}) was taken from Ref. (16 and 17) to be 0.00212 nm at a reference density of 10^{16} cm^{-3}. The major advantage of using this line is that the line is optically thin and therefore not affected by the plasma inhomogeneity [16,17]. Estimation of the absorption coefficient of Al II at 281.62 nm based on the procedures described by Colon[13], reveals a negligible value (0.25 cm^{-1}) for the density range between 10^{17} and 10^{18} cm^{-3}. But for Al II at 466.3 nm, the parameter (w_{ref}) was taken from Ref. (15) to be 0.00685 nm at a reference density of 10^{17} cm^{-3}.
Finally, Figure 7 shows the calculated electron density of the produced plasma in the present work at different delay times (1-7μs) and at different laser energies from the Al II lines 281.6 and 466.3 nm respectively.

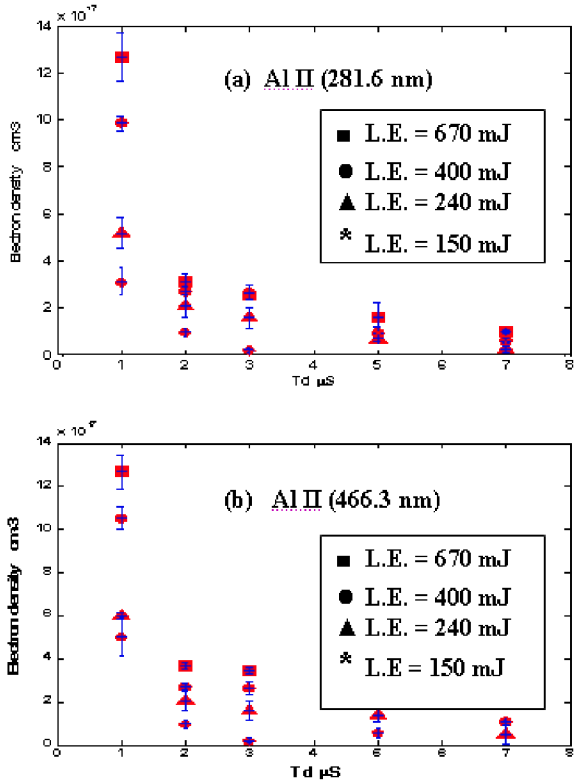

FIGURE 7. Electron density determined from both lines of Al II at (a) Al II 281.6 nm and (b) Al II 466.3 nm versus delay time, for different laser energies.

Fig.(8) and Fig.(9) show the comparison between values of the electron density calculated using the three spectral lines H_α at 656.27 nm, and Al II at 281.6 nm and 466.3 nm. It can be seen that the density determined from both Al II spectral lines are in a good agreement with the density determined from H_α line.

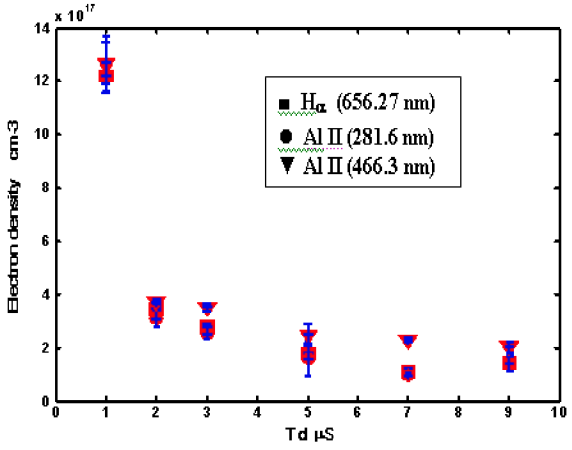

FIGURE 8. Electron density determined from lines of Hα at 656.27 nm, Al II at 281.6 nm and Al II at 466.3 nm at laser energy = 670 mJ for various delay times.

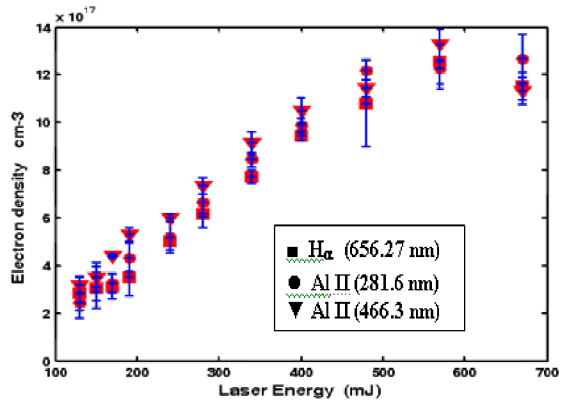

FIGURE 9. Electron density determined from lines of H_α at 656.27 nm, Al II at 281.6 nm and Al II at 466.3 nm for various laser energy, at a delay time of 1 μs.

Finally, the calculated electron densities are in the range of (0.37–1.15) x10^{18} cm^{-3} at laser energies between 130 mJ and 670 mJ for 1 μs delay time. Furthermore the electron densities are in the range between 1.2 x 10^{18} and 0.22x 10^{18} cm^{-3} at different delay times between 0 and 9 μs for laser energy at 280 mJ. These results indicate that the electron density at the initial stage is very high and decreases quickly with time. After the end of the laser pulse, the atoms in the plasma are excited and ionized constantly while leaving the target surface and traveling in the direction of the laser source. Moreover, the impact excitation and ionization occurring after the end of the laser pulse are the dominant processes in the plasma. Higher laser energy gives rise to more target heating and vaporization, resulting also in a higher vapor density as expected.

CONCLUSION

The resultant excitation temperatures increase with increasing the laser energy while they decrease with increasing the delay time. Moreover the electron densities increase with increasing the laser energy while they decrease with increasing the delay time. The results demonstrated that temperature and electron density depend strongly on the delay time and on the laser energy. It can be seen that the density determined from both Al II spectral lines are in a good agreement with the density determined from H_α line.

REFERENCES

1. D.A. Rusak, B.C. Castle, B.W. Smith and J.D. Crit. *Rev. Anal. Chem.* **27,** 257– 290 (1997) .
2. K. Song, Y.I. Lee and J. Sneddon, *Appl. Spectrosc. Rev.* **37**, 89– 117. (2002)
3. E. Tognoni, V. Palleschi, M. Corsi and G. Cristoforetti, *Spectrochim. Acta, Part B*, **57** 1115–1130 (2002).
4. J.M. Vadillo and J. J. Laserna, *Spectrochim. Acta, Part B*, **59,** 147– 161.(2004).
5. J. Sneddon and Y. I. Lee, *Spectrometry, Anal. Lett.* **32,** 2143– 2162 (1999).
6. W. B. Lee, J. Wu, Y. I. Lee and J. Sneddon, *Appl. Spectrosc. Rev*. **39**, 27– 97 (2004).
7. L.J. Radziemski and D. A. Cremers, "Spectrochemical analysis using laser plasma excitation", in: L.J. Radziemski and D.A. Cremers (Eds.), "Laser-Induced Plasmas and Applications", Chap. 7, Marcel Dekker, New York, 1989, pp. 295– 325.
8. Y.W. Kim, "Fundamentals of analysis of solids by laser-produced plasmas", in: L. J. Radziemski and D.A. Cremers (Eds.), "Laser-Induced Plasmas and Applications", Chap. 8, Marcel Dekker, New York, 1989, pp. 327– 346.
9. Y. I. Lee, K. Song and J. Sneddon, "Lasers in Analytical Atomic Spectroscopy", Chap. 5, VCH Publishers, New York, (1997) pp. 197– 235.
10. O. Barthe´lemy, J. Margot, S. Laville, F. Vidal, M. Chaker, B. Le Drogoff, T.W. Johnston and M. Sabsabi, *Appl. Spectrosc.* **58,** 122 (2004).
11. A.M. El Sherbini H. Hegazy, Th. M. El Sherbini, *Spectrochimica Acta Part B* **61,** 532- 539 (2006).
12. A. Escarguel, B. Ferha, A. Lesage and J. Richou, **64** 353-361 (2000).
13. C. Colon, G. Hatem, E. Verdugo, P. Ruiz, J. Campos, *J. Appl. Phys.* **73** , 4752–4758 (1993).
14. H. Hegazy, OI Spectral Line for Diagnostics of the Laser Induced Plasma in Air, sent for publication.
15. A. W. Allen, M. Blaha, W. W. Jones, A. Sanchez, and H. R. Griem, *Phys. Rev. A* **11**, 477 (1975).
16. Lochte Holtgreven W., "Plasma Diagnostics", AIP Press American Institute of Physics, New York, 1995. Originally published by North-Holland Publishing Company, 1995.
17. V. Detalle, R. Heon, M. Sabsabi and L. St-Onge, *Spectrochim. Acta Part B* **56** 1011–1025 (2001).